Journal of Structural Geology 37 (2012) 236–247

Contents lists available at SciVerse ScienceDirect

Journal of Structural Geology

journal homepage: www.elsevier.com/locate/jsg

Geometric curvature analysis of intersecting kink bands: A new perspective on the 3D geometry of kink folds

Rachel E. Dunham [a,*], Juliet G. Crider [b]

[a] Department of Geology, Western Washington University, 516 High Street, MS 9080, Bellingham, WA 98225, USA
[b] Department of Earth and Space Sciences, University of Washington, Box 351310, Seattle, WA 98195, USA

ARTICLE INFO

Article history:
Received 27 May 2011
Received in revised form
22 December 2011
Accepted 18 January 2012
Available online 28 January 2012

Keywords:
Kink bands
Geometric curvature
Fold intersections
Laser scanning

ABSTRACT

We describe a complex set of monoclinal contractional kink bands, exposed in outcrops of the Darrington Phyllite on Samish Island, northwestern Washington, using traditional field measurements and differential geometry. This study is the first to apply laser scanning and geometric curvature analysis to kink bands to obtain a quantitative description of band geometry on the foliation surface. Kink bands in cross section have straight, parallel boundaries that deform a well-defined foliation; in plan view, however, kink band hinges curve and anastomose across the foliation surface, and adjacent bands commonly intersect. Three types of intersections are common: crossing (X), bifurcating (Y), and obliquely diverging (λ); many kink bands also taper out along strike. Geometric curvature analyses were performed on millimeter-resolution DEMs of hand samples containing intersecting kink bands. Maps of curvature parameters (e.g. mean curvature, geologic curvature) clearly outline kink bands in the samples and illuminate the geometry of kink band hinges in each type of intersection. Shortening across hand samples varies where kink bands intersect. Correlations among geometric parameters corroborate rigid rotation as a kinking mechanism for these bands. Quantitative geometric description is the first step toward understanding the three-dimensional mechanics of kink bands.

1. Introduction

Differential geometry has been shown to be a powerful tool in quantifying the three-dimensional geometry of complex surfaces and predicting areas of highest strain (e.g. Lisle, 1994; Stewart and Podolski, 1998; Bergbauer and Pollard, 2003; Pearce et al., 2006; Mynatt et al., 2007; Stecchi et al., 2009; Lisle et al., 2010). Curvature analyses can uniquely describe the shape of a folded surface (e.g. Lisle and Robinson, 1995; Bergbauer and Pollard, 2003), relate the strain distribution within a fold to the location and orientation of fractures and joints (e.g. Bergbauer and Pollard, 2004), and determine the concentration of maximum three-dimensional strain (e.g. Pearce et al., 2006). Quantifying the shape of a surface and calculating the unique parameters for each point on that surface can provide insight into the distribution and localization of strain in folded rocks and may aid in understanding the relationships among adjacent structures.

This study is the first to apply geometric curvature analyses to kink bands. We analyze a complex set of intersecting kink bands in order to produce quantitative descriptions of kink band morphologies and of their relationships to one another. Kink bands are a distinct type of double-hinged fold that are traditionally viewed in simple two-dimensional cross section (e.g. Dewey, 1965, Fig. 1) but can have complex forms on the foliation surface. The curving, anastomosing, and intersecting geometry of kink bands in the third dimension can be described qualitatively using outcrop/surface maps and written descriptions (e.g. Verbeek, 1978; Kirschner and Teixell, 1996), but quantitative descriptions of the third dimension have not been previously presented. Geometric curvature analyses can quantify the magnitude of curvature of a kink band, outline inflection points and hinges for kink bands, and aid in quantifying the amount of shortening the rock has undergone. More importantly, high-resolution micro-topography coupled with curvature analysis also illuminates the characteristics of kink bands that intersect, merge or split, taper out, or end diffusely. To better illuminate the geometry of intersecting kink bands, curvature analyses were performed on samples from a well-developed set of kink bands that expose complex patterns on the foliation surface.

* Corresponding author. Tel.: +1 650 207 0908.
E-mail address: rachel.dunham@gmail.com (R.E. Dunham).

0191-8141/$ – see front matter © 2012 Elsevier Ltd. All rights reserved.
doi:10.1016/j.jsg.2012.01.003

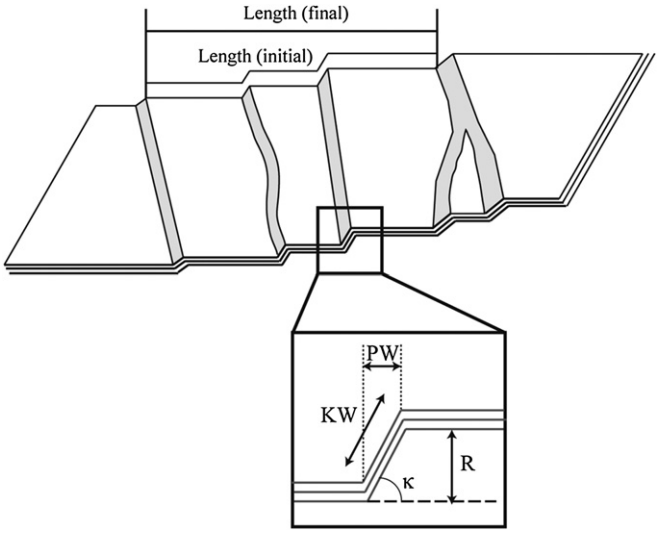

Fig. 1. Schematic representation of kink bands and measured geometric parameters. The top view shows a kinked surface with four kink bands and the final and initial lengths of the surface used for shortening calculations. The inset illustrates the variables discussed in the text: relief (R), rotation angle (κ), kinked width (KW), and plan or peak width (PW). Plan width and hinge width are measured on transects across contour maps of total curvature (see Fig. 4b).

2. Kink bands on Samish Island

Kink bands are well exposed in outcrops of the Darrington Phyllite on Samish Island, northwestern Washington, USA (Fig. 2a). The Darrington Phyllite comprises Jurassic metasediments that have undergone blueschist-facies metamorphism and several subsequent deformation events (Misch, 1966; Haugerud, 1980; Haugerud et al., 1981; Brown, 1986; Gallagher et al., 1988). Kink bands within the phyllite have been noted in several locations throughout the North Cascades (Haugerud, 1980; Haugerud et al., 1981), but the highest concentration of kink bands is on Samish Island, exposed in coastal outcrops and in a reclaimed quarry (Fig. 2a). The structural history of Samish Island is multistage and complex, with at least four folding and/or faulting events prior to kink band development (Lamb, 2000; Schermer et al., 2007). No pervasive deformation has occurred post-kinking, though gentle open folding across the island is possible (Lamb, 2000; Dunham, 2010).

The kink bands of Samish Island deform a steeply south-dipping foliation and comprise a dominantly monoclinal set, with axial planes consistently dipping moderately northeast; a small subset of kink bands have axial planes dipping steeply southwest (Fig. 2b). The majority of kink bands have axial planes at 60°–80° to the foliation (Dunham et al., 2011). The sense of displacement is consistently top to the northeast, even for crossing kink bands; true conjugate kink bands are very rare (only 4 pairs observed). There is some evidence for cross-cutting relationships between the two sets of kink bands, with the southwest-dipping kink bands cutting the northeast-dipping set in one outcrop; however, we interpret the majority of kink bands to be contemporaneous. The kink bands are generally very narrow, with kinked widths commonly less than 1 cm, and are closely spaced at 3–4 cm; a small subset of kink bands have widths up to 2 cm and spacing >50 cm. Shortening was calculated perpendicular to the main kink trends following Ramsay (1967); shortening across individual bands is less than 3% for the majority of kink bands (maximum <10%) and less than 5% for outcrops up to 1.2 m across.

Previous work on the kinematic evolution of kink bands suggests the two likely models of kink band development are a mobile-hinge model (e.g. Paterson and Weiss, 1966; Weiss, 1980; Stewart and Alvarez, 1991) and a fixed-hinge model (e.g. Dewey, 1965; Hobson, 1973; Verbeek, 1978) or some combination thereof. The mobile hinge end-member hypothesis allows kink bands to accommodate shortening by incorporating new material as the hinges migrate outward into the external (undeformed) medium, while the angular geometry of the kink band is fixed at initiation. The fixed hinge hypothesis posits that kink-band width is set at initiation of the kink band, and the structure accommodates strain via rigid rotation of the internal foliation, accompanied by dilation. Based on the geometric properties of the kink bands in cross

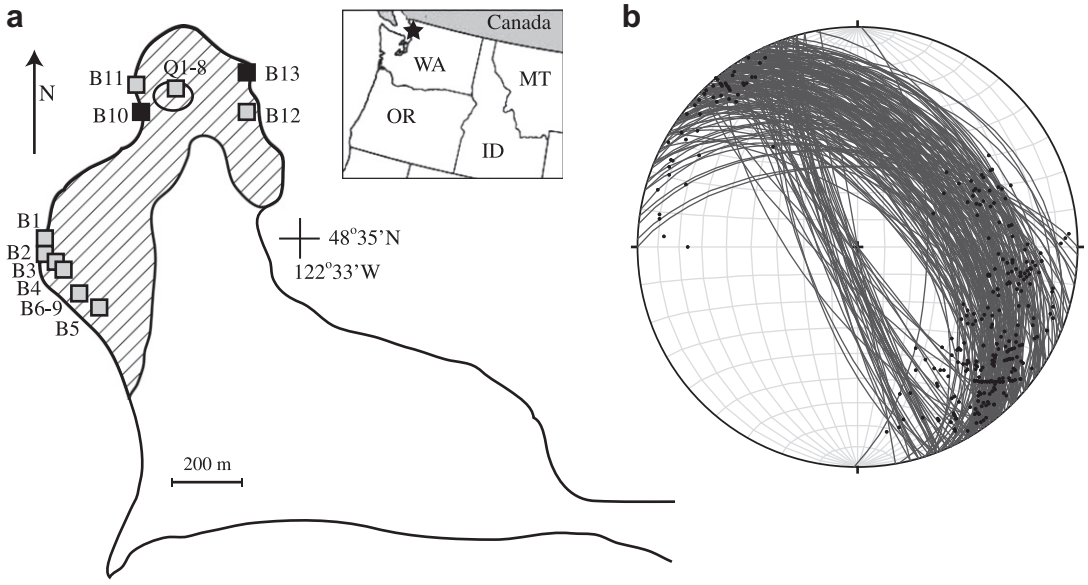

Fig. 2. (a) Schematic geologic map of Samish Island; location within Washington state is shown by the black star on inset. Jurassic bedrock (Darrington Phyllite; hachured area) is exposed only on the northern point of the island as beach outcrops and in a quarry (circle); the remainder of the island consists mainly of Quaternary glacial deposits. Locations where detailed field measurements were made are marked with gray squares; hand samples for curvature scanning were acquired at outcrops marked with black squares. Geologic contact from Jones (1999). (b) Equal area plot of kink band axial plane orientations (great circles) for 210 kink bands and hinge line orientations (points) for 316 kink bands.

section (e.g. the angles between the kink band boundaries and the foliation inside and outside the kink bands, kink bands widths, etc.), the ubiquitous presence of void spaces and veins associated with the kink bands, and microstructures observed in thin section, we conclude that rotation within fixed hinges was the dominant mechanism of kink band formation in this location (Dunham et al., 2011).

In cross section, kink bands are generally straight and parallel, are inclined to the foliation at high angles, and have dominantly "S" asymmetry when viewed down plunge (Fig. 3a). Most outcrops do not expose intersections in this plane; where present, bifurcating (*Y*) and crossing (*X*) intersections are observed and multiple intersections are common (e.g. Fig. 3a). Inspection of crossing kink bands indicates that these intersections do not mark the presence of conjugate kink bands, as both crossing kink bands have the same "S" asymmetry.

On the foliation surface, kink bands commonly intersect due to curving or non-parallel trends of adjacent kink bands (Fig. 3b, c). Three types of intersections are visible: crossing (*X*), bifurcating (*Y*), and obliquely diverging (λ). (Here we use "bifurcate" and "diverge" purely as geometric descriptors and do not imply temporal development.) The most common intersections are Y-type, followed by λ, and finally *X*. True crossing kinks are uncommon. In many places it is difficult to distinguish Y-type from X-type intersections due to the very fine scale of the foliation and weathering that obscures the true path of a single kink band. In some places, a kink band will bifurcate and subsequently rejoin into a single kink band several centimeters away, creating a lozenge-shaped zone of unkinked material between the bifurcated lines (Fig. 3d). In most λ-type intersections the diverging kink band is thinner than the continuous kink band and diverges at a low angle (Fig. 3c), generally tapering out within 10 cm; however, the detailed hinge geometry is difficult to observe at the outcrop. All three types of intersections occur in proximity to each other in many outcrops (e.g. Fig. 3b), further supporting the interpretation of a single kinking event producing the complex patterns. The abundance of intersections and anastomosing kink band trends on the foliation surface can be challenging to describe with traditional techniques. Geometric curvature analyses on millimeter-scale DEMs of hand samples better illuminate the geometry of kink bands and fold hinges within the different types of intersections.

3. Geometric curvature calculations

3.1. Methodology

3.1.1. Data acquisition and refinement

Eight hand samples containing kink bands from Samish Island were selected for surface curvature modeling. The selected rocks came from two outcrops, B10 and B13 (see Fig. 2) and the small beach just south of outcrop B10. Samples were chosen that had cleaved parallel to the foliation, with ideal or intriguing kink band

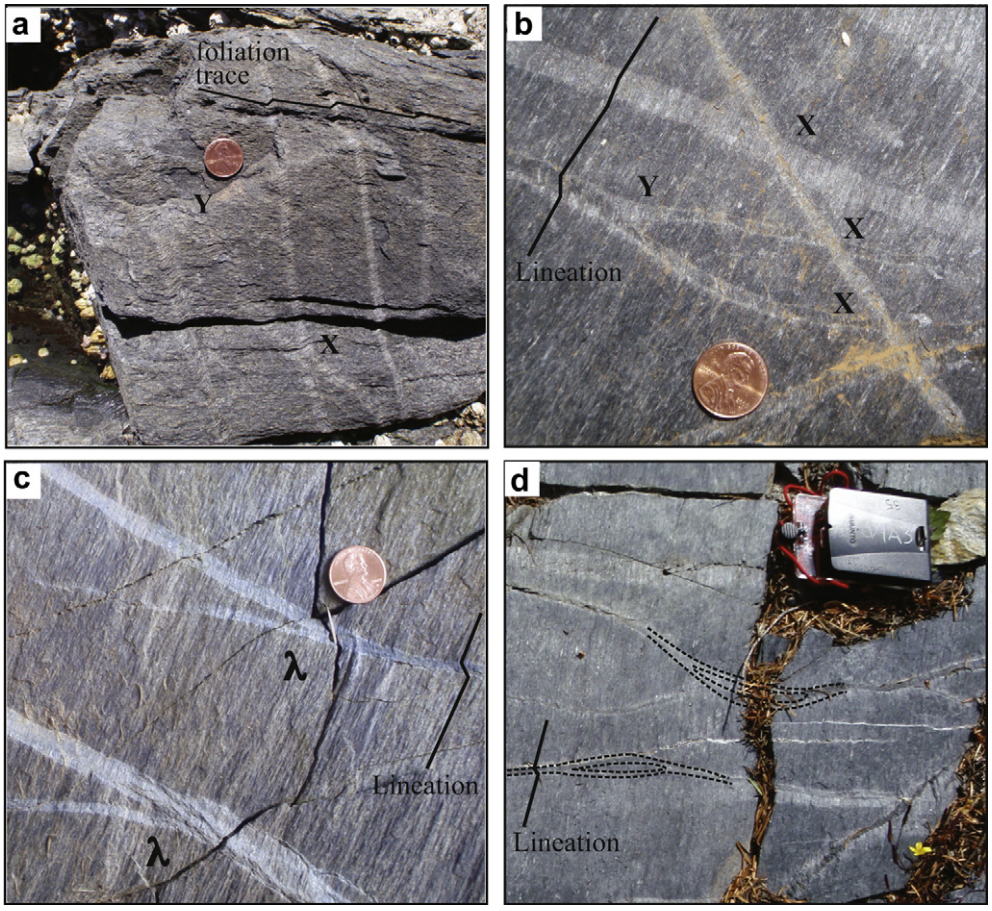

Fig. 3. Kink band geometries in the field. (a) View of kink bands in cross section. Kink bands in this 2D view are relatively straight and narrow and run roughly parallel to each other; rare *X* and *Y* intersections are visible. (b) Crossing (*X*) and bifurcating (*Y*) intersections in close proximity to each other in one outcrop. (c) Two oblique (λ) intersections in two parallel kink bands. Both secondary bands have similar trends and angles with the primary bands. (d) Dashed lines outline the traces of two kink bands that bifurcate and rejoin within several centimeters, forming a lozenge-shaped zone of unkinked material between the two strands.

geometries and intersections on the foliation surface; most important was the presence of a single foliation plane providing the kinked surface. Samples were scanned using a FARO arm 3D laser scanner to produce a point cloud containing x-y-z coordinates of points on the surface. The raw point clouds were decimated to roughly 1.5 mm horizontal spacing for ease of processing. For each sample, we produced an interpolated gridded surface at 0.5 mm spacing. This grid spacing yields a Nyquist frequency of $\sim$1 mm^{-1} (see Bergbauer and Pollard, 2003) and can resolve undulations in the interpolated surface with a wavelength of $\sim$1 mm. Weathered lineations on the rock surfaces introduce high-amplitude noise into the digital model of the kinked foliation. Low pass filters are commonly employed to remove similar noise from DEMs (e.g. Ritchie, 1995) and have been shown to unmask meaningful patterns in curvature from gridded data of map-scale structures (Bergbauer and Pollard, 2003). Following Bergbauer and Pollard (2003), we twice-filtered the gridded data using a 9-node moving average filter, available in standard software packages (e.g. Yilmaz, 2007). The interpolation and filtering applied to our data likely reduces the calculated maximum curvature values a bit and somewhat broadens the measured hinge widths of very tight kink hinges; however, this processing is essential to extracting the essential forms of the kink bands from the weathered surface.

3.1.2. Curvature calculations

Bergbauer and Pollard (2003) presented a method to accurately quantify the curvature of a folded surface with exact mathematical expressions independent of the coordinate system; this method was refined and expanded by Pearce et al. (2006) and Mynatt et al. (2007). We used the matrix algebra approach of Pearce et al. (2006) and modified MATLAB scripts written by Mynatt et al. (2007) to apply the method of Bergbauer and Pollard (2003) to our data.

A curved surface can be described by a combination of tangent and normal vectors at any point along that surface. The normal curvature at any one point is defined by the curvature of an arbitrary line that lies on that surface, and is directionally dependent; that is, the curvature may have different values for different directions around that single point. The magnitude of curvature on a cylindrical fold is equal to the inverse of the radius of the fold, and the units are inverse meters (e.g. Mynatt et al., 2007). The normal curvature will reach minimum and maximum values in two orthogonal directions, and these values are the principal curvatures, K_1 and K_2 (e.g. Bergbauer and Pollard, 2003). The maximum principal curvature (K_1) and its direction at every point can highlight areas of tightest folding, and paired with the directions of minimum principal curvature can highlight the locations of fold hinges (Pearce et al., 2006).

Other curvature parameters, calculated from these principal curvatures, provide further descriptions of a surface. The Gaussian curvature and mean curvature together provide a quantitative description of the shape of a surface (Pearce et al., 2006; Mynatt et al., 2007; Lisle and Toimil, 2007). The Gaussian curvature (K_G) is the product of the two principal curvatures, and the mean curvature (K_M) is the average of K_1 and K_2. Maps of Gaussian curvature can be used to identify inflection points along a surface (Pearce et al., 2006): where $K_G = 0$, the surface is changing from positive to negative curvature. The shape of the surface can be classified based on the Gaussian and mean curvatures by a criterion called the geologic curvature (K_{GEOL}), which differentiates between synformal and antiformal cylinders and saddles, domes and basins, and planar structures (Mynatt et al., 2007). Departures from these ideal structures can be quantified and subtracted using a curvature threshold filter, which identifies areas with overprinted structures (Mynatt et al., 2007). Plotting the absolute value of the mean curvature allows for comparison of the curvature values for adjacent folds of opposite senses (e.g. anticline/syncline) to confirm whether there are consistent curvature values (and thus fold form) for the folds in a pair. However, if the sum of the principal curvatures is close to zero, the mean curvature for those points will also be zero, masking the possibility of significant strain (Stewart and Podolski, 1998). To mitigate the muting effect of K_M, Stewart and Podolski (1998) proposed using the total curvature (K_T), where: $K_T = |K_1| + |K_2|$. Maps of total curvature describe the shape of surfaces better than mean curvature where strain is variable in a small area and surface curvature changes rapidly.

We produced contour plots of these curvature parameters for each sample. We applied a curvature threshold filter to enhance the expression of kink bands in the curvature plots. The threshold filters broad warping of the foliation surface, treating surfaces with curvature values below the threshold as planar (Mynatt et al., 2007). The application of a curvature threshold also allows the surface to be characterized by idealized shapes, such as antiforms and perfect saddles. We chose an initial threshold value of $\sim$0.1 mm^{-1}, corresponding to a curvature value much smaller than the average curvature of the kink band hinges. The value was adjusted manually for each sample to reduce the expression of noisy surface topography without suppressing the more subtle kink bands or small features. This compromise permits some noise in order to preserve more of the structure.

Relative elevation, gradient, and curvature data were extracted across multiple transects along each sample surface. Transect lines were drawn parallel to the lineation and approximately perpendicular to the kink band hinges. Kink bands were identified on a graph of distance along the transect versus gradient and curvature (Fig. 4) and by comparing the transect to a map of the sample. Data for each kink band along a given transect were manually extracted. Careful interpretation is required in order to correctly identify the true deformation features, as irregular surface shapes can imitate the fold signals. Kink bands are distinguished in the transect lines by a steep peak in values of gradient accompanied by sharp peaks in curvatures that directly coincide with the edges of the gradient peak (Fig. 4b). The curvature peaks always consist of synclinal–anticlinal pairs that match the step-sense of the sample. Plan width (PW; see Fig. 1) of kink bands and the width of band hinges (HW) are measured on these profiles. Plan width is the horizontal width of the kink band along the transect line, measured as the distance between peaks in total curvature of the hinges; hinge width is the width of the hinge zone, measured as the base with of each peak in hinge curvature (Fig. 4b). Extracted values were used for statistical calculations and to evaluate correlations among these attributes.

4. Curvature maps and analyses

Contour maps of surface topography, gradient, and curvature parameters for each sample indicate that the methods outlined above accurately capture the expression of kink bands on the foliation surface, and that these methods can be used to describe kink bands quantitatively as well as qualitatively. A photograph of a scanned sample and associated maps of gradient, mean curvature, total curvature, and geologic curvature are shown in Fig. 5a, b, c, d, and e, respectively. Image sets for all samples are available as an electronic supplement to this paper.

4.1. Kink band expression

Kink bands are well expressed in maps of gradient (Fig. 5b), where zones of similarly steep slopes represent kink bands, surrounded by relatively flat surfaces. Gradients of kink bands range

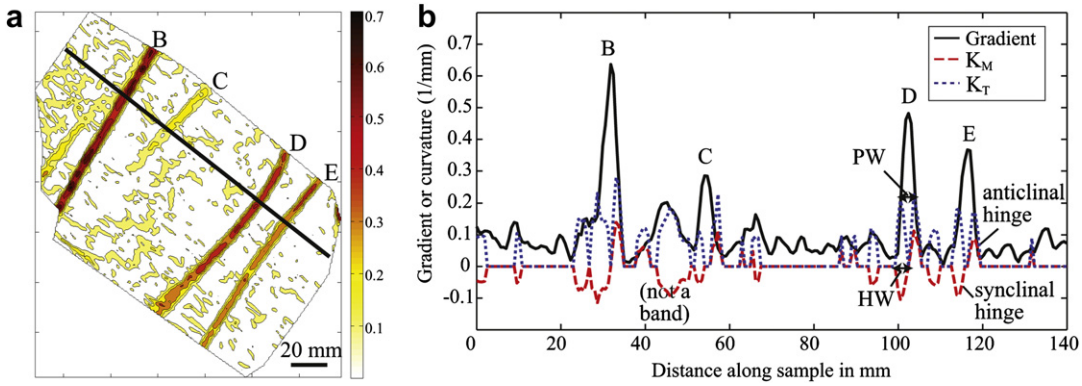

Fig. 4. Example transect location and extracted data, sample B10-F4. (a) Gradient map, where zones of high gradient mark the kink bands. (b) Gradient peaks in the transect data corresponding to kink bands are well above background and are accompanied by a peak-trough pair in the mean curvature data (K_M). The order of the peak-trough set is dependent on the step-sense of the sample; in this sample, kink bands step up from left to right, so kink band peaks have synclinal (trough) – anticlinal (peak) hinges from left to right. Four bands are visible in this transect. K_T is total curvature. Plan width (PW) and hinge width (HW) are measured as shown.

from ~0.2 up to 0.8 (average: 0.25–0.3), and most samples show a wide variety of gradients among the kink bands. Within individual kink bands, the gradient usually remains approximately constant throughout the kink band, except where kink bands split, merge, or bend (see Section 4.2). The sample shown in Fig. 5a has three straight kink bands and two that bend toward each other; kink band B is straight and narrow with a consistent gradient of ~0.6 along its length. In contrast, kink bands D and E have different gradient values at the nose of the bend (D increases from 0.4 to 0.5 and E decreases from 0.45 to 0.35), indicating that deviation from a straight trajectory influences the steepness of the kink band. The steepness of the kink band is also linked with the sharpness of the kink band hinges; kink bands with steeper kinked planes (higher gradients) usually have well-defined boundaries (e.g. band B in Fig. 6b), whereas gentler or very wide kink bands have wide or even diffuse boundaries, and can be difficult to distinguish from the generally flat background.

Contour plots of curvature parameters (Fig. 5c, d, and e) best illuminate the location and geometry of kink band hinges. Most kink bands have paired hinges of equal widths, with higher curvature values at the center of the hinge zone (Fig. 5c). Curvature values are generally constant along the hinges and between paired

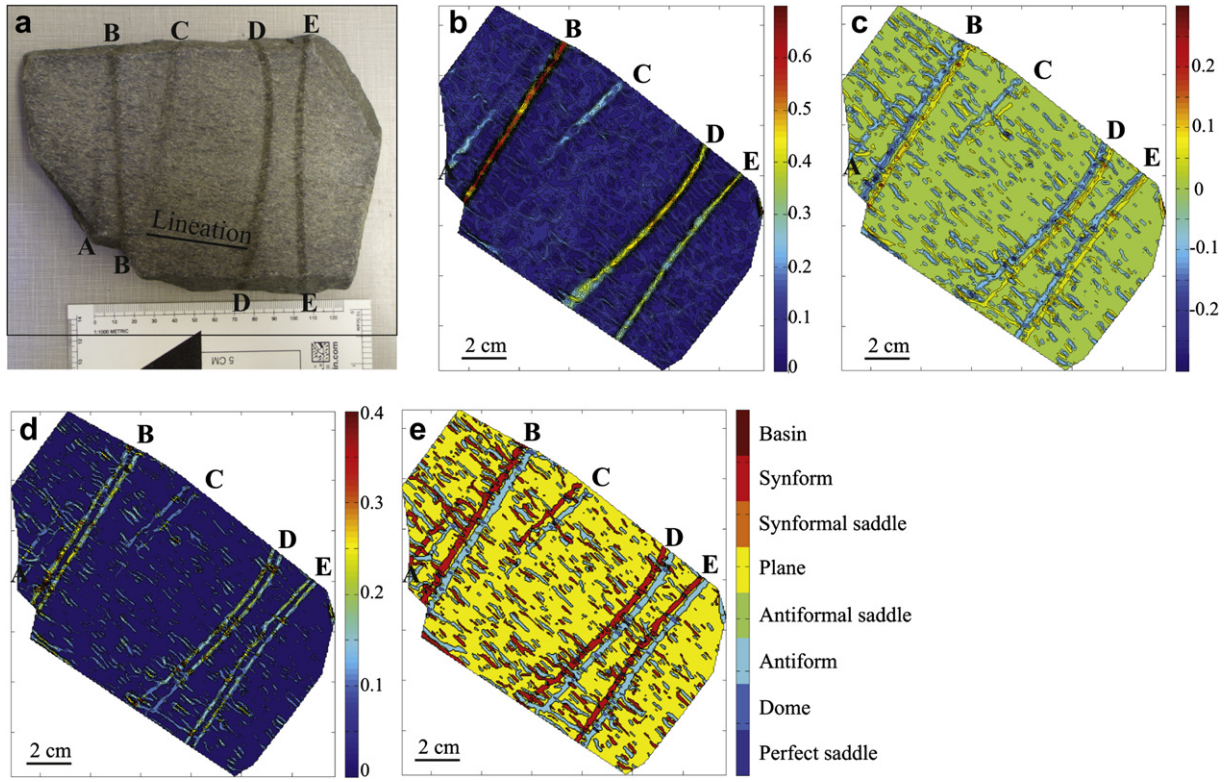

Fig. 5. Curvature analysis output for sample B10-F4. (a) Annotated photograph of the sample, followed by contour maps of (b) gradient, (c) mean curvature (mm^{-1}), (d) total curvature (mm^{-1}), and (e) geologic curvature. Streaking perpendicular to kink bands in curvature maps is the residual signal from the mineral lineation that passed through the applied filters. Geologic curvature classification after Mynatt et al. (2007).

hinges (Fig. 5c, d), similar to the constant gradient along each band. Zones of negative curvature identify synformal hinges (compare Fig. 5c and e), and positive curvature corresponds to antiformal hinges. Each pair of hinges bracket a planar (zero curvature) surface, consistent with the idealized form of a kink band as a planar surface bounded by two tight hinges. Mean curvature of hinges ranges from ±0.05 to ±0.03 mm^{-1}, corresponding to curvature radii of 20 mm–3.3 mm. The higher mean curvature values (generally $|K_M| > 0.15$ mm^{-1}) at the center of the hinges mark the sharp bend of the foliation that is easily visible in hand sample and correspond to the tight, narrow hinge zones outlined by the total curvature (Fig. 5d). The lower mean curvature values for the rest of the hinge zone suggest that kink band hinges are not single sharp lines but instead narrow strips of increased curvature. Resolution of further details in variation within and along the hinges is limited by the data density and smoothing filters applied to the data. The geologic curvature (Fig. 5e) indicates that each kink band is indeed composed of a synform-plane-antiform set as indicated by the gradient and curvature maps, and confirms that the bands comprise a monoclinal set, with the same stepwise sequence for all kink bands within a particular sample. The successful simplification of the kink bands into these idealized fold shapes via the threshold curvature value indicates that kink band hinges can indeed be approximated by cylindrical folds.

4.2. Kink band intersections

Field investigation identified three types of kink band intersections in the Samish Island outcrops: crossing (X), bifurcating (Y), and obliquely diverging (λ). All three types of intersections are present in the scanned samples, and multiple intersections occur within a single kink band group. Each intersection type has unique features present in the curvature maps, and identification of these diagnostic features may aid in interpreting more complicated surfaces. Photographs, gradient and curvature maps for each type of kink band intersection are given in Figs. 6–8.

4.2.1. Crossing (X) intersections

Three X-type intersections were scanned; in all three instances the sense of kink displacement is consistent for both kink bands, so none of the crossing sets of kink bands can be considered a conjugate set. All three X intersections have acute angles of 25–38° and obtuse angles of 130–150°, and there is typically a ~5° difference for paired acute angles for a single intersection. Where the two kink bands cross, a distinct rhomb-shaped patch can be observed in hand sample (Fig. 6a), clearly kinking at a different angle than either kink band external to the intersection. The gradient of the rhomboid patch is much higher, up to twice as steep as that of either kink band: in Fig. 6b, kink band B has an average gradient of 0.55 compared to ~0.35 for kink band C, the sum of which is comparable to the very steep (>0.8) gradient within the rhomb intersection. Where crossing kink bands are thinner, more extreme contrast is seen at the intersection; kink band width appears to have an effect on the magnitude of slope change at a crossing intersection.

Maps of mean and total curvature (Fig. 6c, d) show knots of elevated curvature where the hinges of one kink band cross the other. Contour plots of total curvature outline the traces of the kink bands especially well, clearly marking the rhomb of combined kink bands and highlighting the clusters of high curvature at the crossing of the hinges (K_T >0.3 mm^{-1} at the vertices versus <0.25 mm^{-1} outside). These knots of curvature correspond to the vertices of the rhomboid patch described above. The magnitude of each knot is dependent on the combination of hinges interacting at each point: antiformal–antiformal, synformal–synformal, or antiformal–synformal. Where two hinges of the same sense (antiformal or synformal) cross, curvature values reach extremes, up to twice as high as outside the intersection. An antiformal–synformal combination results in lower and sometimes almost negligible mean curvature, and the opposing sense of folding results in an apparent flattening of the hinge zone. These changes in mean curvature at the rhomboid intersection are reflected in the geologic curvature (Fig. 6e): two antiformal hinges

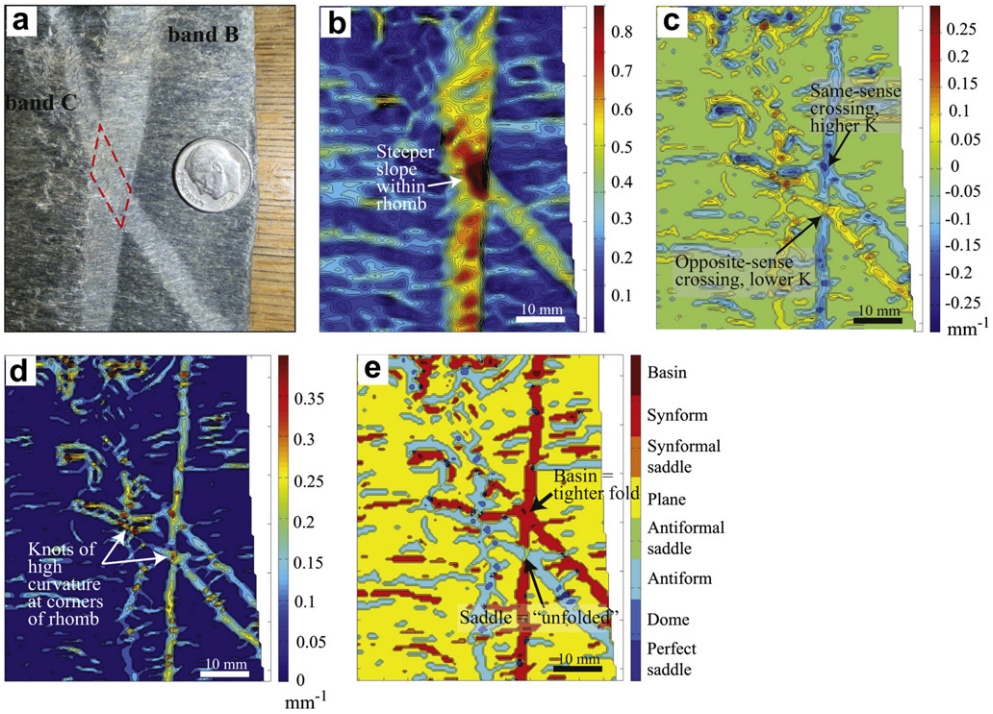

Fig. 6. Complete set of curvature maps for an X-type intersection. (a) Photograph of the intersection on the sample, with bands labeled and the rhomb intersection outlined. The intersection rhomb is visible in plots of (b) gradient, (c) mean curvature, (d) total curvature, and (e) geologic curvature.

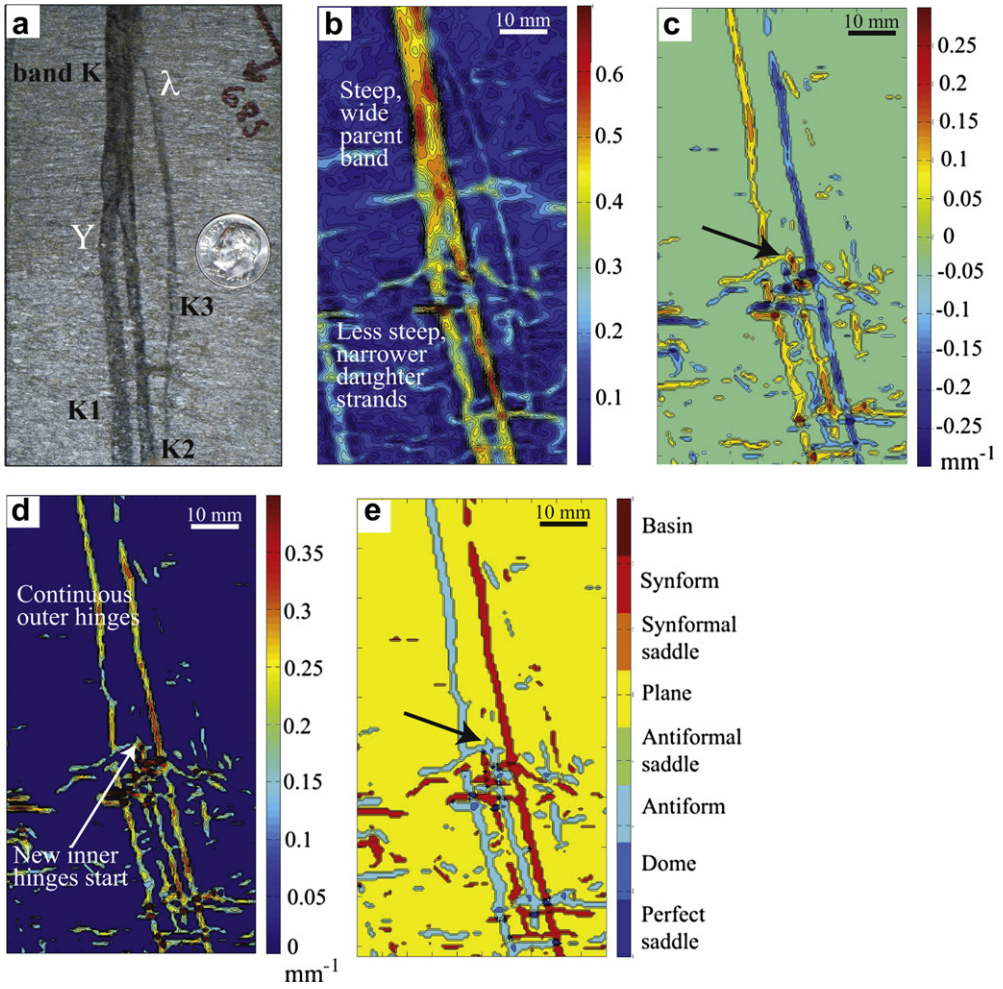

Fig. 7. Complete curvature maps for a *Y*-type intersection. (a) Photograph of the intersection on the sample, with bands and *Y* intersection labeled; notice a *λ*-shape intersection occurs near the top of the band. The fork-like nature of the splitting band is visible in plots of (b) gradient, (c) mean curvature, (d) total curvature, and (e) geologic curvature. The location of the new hinges is marked by arrows.

crossing form a dome, a synformal pair forms a basin, and crossing hinges of opposing fold senses appear as saddles. The sense of the saddle (synformal or antiformal) is dependent on the shape of the dominant hinge (the hinge that is most continuous and has higher overall curvature is dominant). Crossing intersections are easily recognized in hand sample and have distinct curvature and surface shapes, synthesized in Fig. 9a.

4.2.2. Merging/bifurcating (Y) intersections

Seven *Y* intersections were identified in three scanned samples. True *Y* intersections are fork-like, with a single parent kink band splitting symmetrically into two smaller kink bands (Fig. 7a); in two places, two *Y* intersections occur within a single kink band, splitting and rejoining to create a lens of unkinked material within the composite kink band (similar to the field geometry shown in Fig. 3d). The angle between forked kink bands is very low, commonly around 10°. For all fork-like intersections, the parent kink band is wider than the daughter strands, usually widening slightly just before the fork. The daughter kink bands are generally close to the same width as each other, but significantly thinner than the parent. The sum of the daughter widths is approximately the width of the single parent kink band. The parent kink band has a steeper slope than the offshoots, with maximum gradient values usually obtained just before the point of the V (Fig. 7b). The slopes of the daughter strands are significantly lower than that of the parent, but similar between the daughters. A wedge of clearly lower gradient (almost background) is visible between the divided strands.

Mean curvature and total curvature (Fig. 7c, d) outline the geometry of the hinges at the intersection, delineating best the fork-like nature of the split. The original kink band's hinges become the outer hinges of the two kink bands of the fork, and two new hinges appear between, forming the inner hinges. The outer hinges bow outwards and remain continuous; the inner hinges initiate at a point as thin tapered zones, but quickly widen to approach the width of the outer hinges. The outer hinges also retain similar curvature values from the parent kink band, and the inner hinges have lower magnitude curvature values at their start (barely above background) before tightening to match the outer hinges. Knots of elevated curvature are common on the outer hinges just as they begin to split and bow outwards from the parent band. Geologic curvature (Fig. 7e) reveals no distinct or unique shape to the point of bifurcation or to the nucleation of new hinges.

Y-type intersections occur when two kink bands merge or split at low angles, and they have curvature and geometric properties that are clearly distinct from X-type intersections (Fig. 9b). It is unclear whether the dominant method of formation is merging of two kink bands into one or bifurcation of a parent kink band into

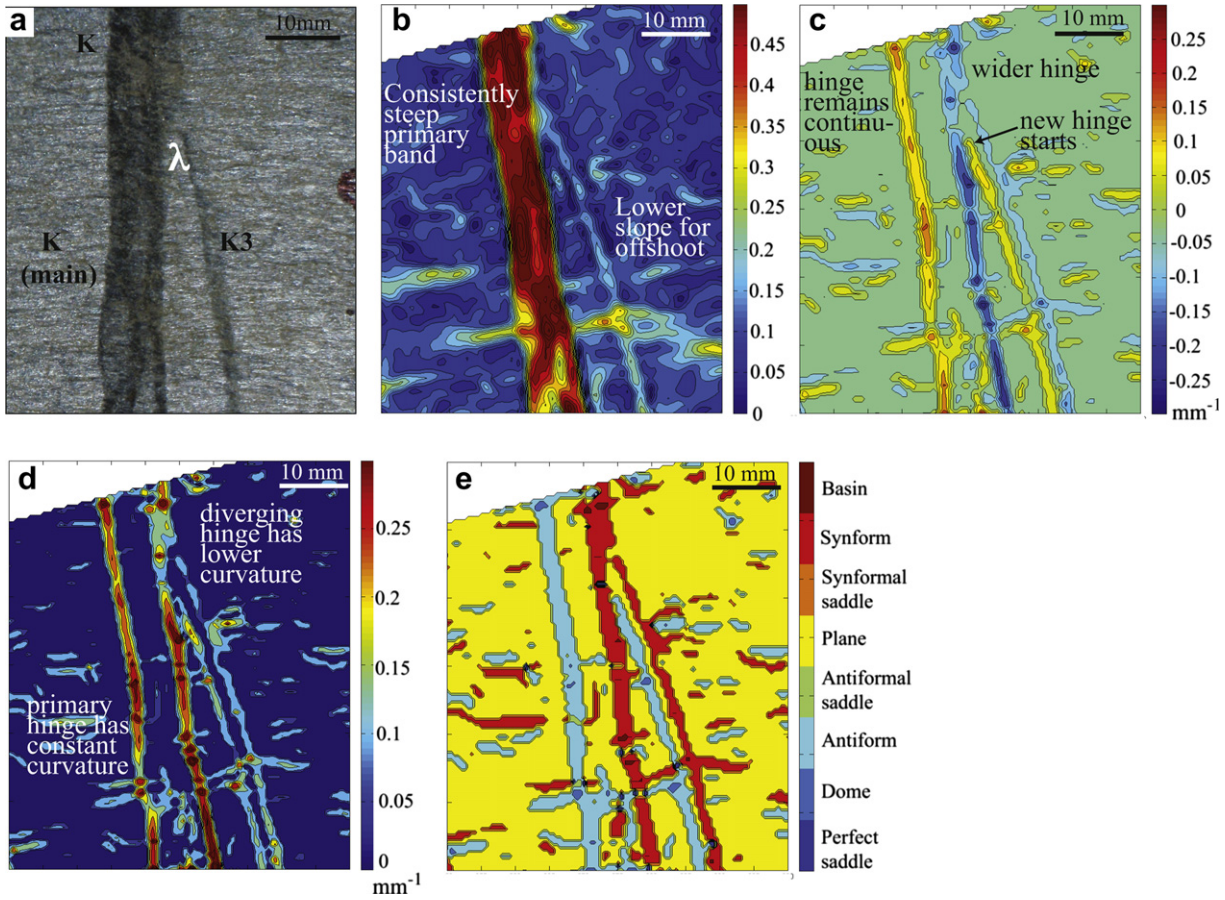

Fig. 8. Complete curvature maps for a λ-shape intersection. (a) Photograph of the intersection on the sample. The secondary band is subordinate to the primary band but still clearly visible in plots of: (b) gradient, (c) mean curvature, (d) total curvature, and (e) geologic curvature.

two strands, and the control(s) on why and where Y-type intersections occur are similarly unknown.

4.2.3. Obliquely diverging (λ) intersections

Kirschner and Teixell (1996) describe T-type intersections as the truncation of one kink band by another, inferring that the abutting kink band was younger and was stopped in its development by the older, truncating kink band. True truncation would require that the hinges of the abutting kink band would stop abruptly at the truncating kink band, with no visible connection to the truncating kink band's hinges. The abutting band would also show a decrease in relief toward the point of truncation, as observed by Kirschner and Teixell (1996). The majority of kink band intersections in the samples from Samish Island do not show total truncation of the abutting kink band; instead, one hinge from the primary kink band appears to split (or merge) while the other primary hinge remains continuous and straight, in a hybrid Y-T intersection that may more appropriately be described as a "λ-shape" intersection (Fig. 8a). This geometry is not always clearly visible in hand sample, and close examination of curvature plots illuminates the distinct geometry of the hinges. Field observations reveal that the secondary kink band generally tapers out within a few centimeters of the intersection, in contrast to the observations presented by Kirschner and Teixell (1996).

λ-type intersections are the most abundant of all intersection types in the scanned samples, with at least 8 and possibly 12 examples in three rocks. λ intersections are characterized by a thin (secondary) strand diverging from one hinge of a wider primary kink band (Fig. 8a); the offshoots are much thinner and less pronounced than the primary kink band. Gradient plots confirm that the offshoots have much lower slopes than the primary kink bands, usually barely above background levels (Fig. 8b). The primary kink band retains relatively constant slopes along its length despite the small offshoot.

The geometry of kink bands involved in λ intersections is most clearly shown in maps of mean and total curvature (Fig. 8c, d). For all clear λ intersections, the primary kink band does not split as a whole, nor does the secondary kink band fully truncate its hinges against the main band. Instead, one hinge of the primary kink band remains continuous and does not change its trend, unlike the *Y* intersections where both kink bands commonly bow outwards at the bifurcation. In a λ-type intersection, the second primary hinge is modified, becoming two: one strand continuous as the primary hinge, usually retaining close to the same width and curvature as the original hinge, whereas the other strand veers off at an oblique angle (usually 20–30°) with slightly lower curvature and a slightly smaller width before becoming subparallel to the hinges of the primary kink band. Where the two hinges begin to split, the overall width of the joined hinge increases slightly. The magnitudes of mean and total curvatures of the splitting hinge in the wider hinge zone are commonly lower than the curvatures of the other primary hinge at that point (e.g. 0.1–0.15 mm^{-1} for the splitting hinge versus >0.2 mm^{-1} for the continuous hinge, Fig. 8c). The second hinge of the secondary kink band begins in the wedge between the split hinges, not at the point of bifurcation itself. The new hinge tapers into existence, starting thin and with low curvature

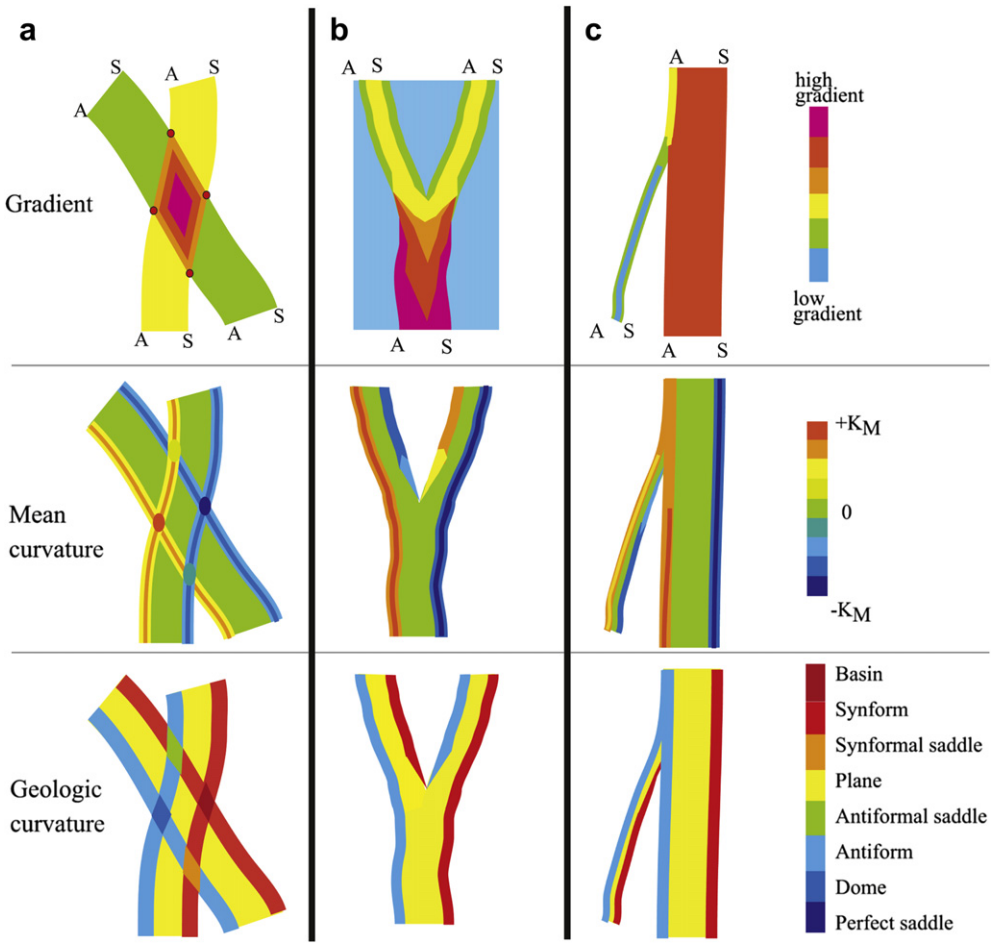

Fig. 9. Illustrations of idealized (a) *X*, (b) *Y*, and (c) *λ* intersections. "A" and "S" denote anticlinal and synclinal hinges, respectively.

(<0.1 mm^{-1} mean curvature and <0.15 mm^{-1} total curvature; Fig. 8c, d), then increasing to match the other secondary hinge. Geologic curvature maps (Fig. 8e) also outline the wider shape in the splitting hinge, and nucleation of a new, thin, separate hinge in the wedge between the split hinges.

λ-type intersections are distinct from Y-type intersections in the widths of the two kink bands involved and the geometry of the hinges at the point of intersections (Fig. 9c). From the scanned samples, *λ*-type intersections appear to be the most common and are better characterized as obliquely diverging (or merging) rather than abruptly truncating. In the field it can be difficult to distinguish *Y* from *λ* intersections, though reexamining photographs and samples after curvature analyses suggests that the two intersections can be distinguished if the geometry of the hinges and two strands are traced based on the curvature results.

4.3. Statistical relationships and shortening

Numerical data for kink bands were extracted along four to six transects across each sample, parallel to the lineation and generally perpendicular to the main kink trend. Data extracted were: spacing between kink bands, plan width of each kink band, relief, hinge curvature, mean gradient, and peak gradient. Mean gradient is the average gradient between the two hinges, and peak gradient is the maximum gradient value for the kink band. As many kink bands as possible were measured on each transect, providing at least one and optimally five or six points of measurements for each kink band in a given sample.

The shortening (-*e*) for each line (Table 1) was calculated using the transect data:

$$-\boldsymbol{e} = \frac{\boldsymbol{L}_{\text{final}} - \boldsymbol{L}_{\text{initial}}}{\boldsymbol{L}_{\text{initial}}} \quad (1)$$

where the final length was measured from the inner hinges of the outermost kink bands, and the initial length was the sum of the intervening spacings and kinked widths (Fig. 1). Lines that cross more kink bands generally have more shortening, indicating that the magnitude of shortening is dependent on the number of kink bands along a line. Thus, strain is distributed among the kink bands, not dominated by individual structures.

To better compare values between samples with different numbers of kink bands, a kink band density (D_{kb}) was calculated for each line:

$$\boldsymbol{D}_{kb} = \frac{\boldsymbol{N}}{\boldsymbol{L}_{\text{final}}} \quad (2)$$

where *N* is the number of kink bands along the line. Shortening values were also normalized to the number of kink bands measured to give an estimate of accommodated strain per kink band. Both types of shortening are shown in Table 1 and were used in correlation computations shown in Table 2. Correlation coefficients (*R* and R^2) for multiple variables were computed to look for meaningful relationships between measured and calculated parameters (Table 2); calculations were performed on individual kink bands as well as all transect averages. The small data set precludes strong

Table 1
Transect shortening data for all six surfaces scanned.

Sample	Transect	Across full length of sample						Across same set of bands for each sample					
		No. of bands	$L_{initial}$ (mm)	L_{final} (mm)	−e	$-e_{norm}$	D_{kb} (cm^{-1})	No. of bands	$L_{initial}$ (mm)	L_{final} (mm)	−e	$-e_{norm}$	D_{kb} (cm^{-1})
B10-1a	1	1	61.60	61.50	0.16%	0.16%	0.16	–	–	–	–	–	–
	2	3	93.99	93.02	1.04%	0.35%	0.32	3	89.27	88.21	1.19%	0.40%	0.34
	3	4	118.00	116.55	1.23%	0.31%	0.34	3	81.52	80.52	1.22%	0.41%	0.37
	4	5	117.20	116.15	0.89%	0.18%	0.43	3	75.02	74.20	1.10%	0.37%	0.40
	5	4	91.78	90.71	1.17%	0.29%	0.44	3	74.34	73.48	1.16%	0.39%	0.41
B10-1b	1	3	110.83	110.34	0.45%	0.15%	0.27	2	81.43	81.27	0.20%	0.10%	0.25
	2	3	109.43	109.01	0.38%	0.13%	0.28	2	81.92	81.76	0.20%	0.10%	0.24
	3	2	84.26	84.04	0.26%	0.13%	0.24	2	84.26	84.04	0.26%	0.13%	0.24
	4	3	117.52	117.20	0.28%	0.09%	0.26	2	83.89	83.71	0.21%	0.11%	0.24
	5	3	113.04	112.63	0.36%	0.12%	0.27	2	82.45	82.22	0.29%	0.14%	0.24
B10-F3	1	4	95.76	95.06	0.73%	0.18%	0.42	3	60.43	59.94	0.81%	0.27%	0.50
	2	9	212.34	210.67	0.79%	0.09%	0.43	3	65.69	65.07	0.95%	0.32%	0.46
	3	9	211.28	209.06	1.05%	0.12%	0.43	2	60.11	59.51	0.99%	0.49%	0.34
	4	11	228.31	225.91	1.05%	0.10%	0.49	3	59.98	59.39	0.97%	0.32%	0.51
	5	10	206.61	204.33	1.10%	0.11%	0.49	3	63.40	62.87	0.83%	0.28%	0.48
	6	9	174.84	172.77	1.18%	0.13%	0.52	4	60.47	59.87	1.00%	0.25%	0.67
B10-F4	1	2	92.15	91.82	0.35%	0.18%	0.22	2	92.15	91.82	0.35%	0.18%	0.22
	2	2	90.48	90.18	0.33%	0.16%	0.22	2	90.48	90.18	0.33%	0.16%	0.22
	3	2	90.51	90.24	0.30%	0.15%	0.22	2	90.51	90.24	0.30%	0.15%	0.22
	4	2	95.37	94.67	0.74%	0.37%	0.21	1	83.49	83.26	0.28%	0.28%	0.12
	5	2	97.54	96.89	0.67%	0.33%	0.21	1	84.10	83.92	0.21%	0.21%	0.12
B13-4T	1	8	195.90	194.11	0.92%	0.11%	0.41	8	195.90	194.11	0.92%	0.11%	0.41
	2	11	312.41	310.60	0.58%	0.05%	0.35	8	202.76	201.51	0.62%	0.08%	0.40
	3	12	312.19	309.97	0.71%	0.06%	0.39	8	203.14	201.58	0.77%	0.10%	0.40
	4	12	308.63	306.76	0.60%	0.05%	0.39	8	202.33	200.98	0.67%	0.08%	0.40
	5	10	278.62	276.21	0.86%	0.09%	0.36	8	203.26	201.56	0.84%	0.10%	0.40
	6	9	268.75	266.78	0.73%	0.08%	0.34	8	207.87	206.20	0.80%	0.10%	0.39
B13-4B	1	12	295.99	294.26	0.58%	0.05%	0.41	10	211.46	210.26	0.56%	0.06%	0.48
	2	12	282.41	280.51	0.67%	0.06%	0.43	10	203.85	202.53	0.65%	0.06%	0.49
	3	15	303.63	301.32	0.76%	0.05%	0.50	12	198.76	197.19	0.79%	0.07%	0.61
	4	13	332.31	330.06	0.68%	0.05%	0.39	10	215.97	214.57	0.65%	0.07%	0.47
	5	12	308.65	306.50	0.70%	0.06%	0.39	9	197.76	196.50	0.64%	0.07%	0.46
	6	10	314.71	312.29	0.77%	0.08%	0.32	7	197.52	196.27	0.63%	0.09%	0.36
Minimum					0.16%	0.05%	0.16				0.20%	0.06%	0.12
Maximum					1.23%	0.37%	0.52				1.22%	0.49%	0.67
Mean					0.70%	0.14%	0.35				0.67%	0.19%	0.37

correlations (i.e. $R^2 > 0.9$); however, meaningful relationships can still be drawn from weaker correlations, recognizing the limitations of the data set. A threshold of $R^2 > 0.5$ was used to identify correlations in the curvature data, and the results were compared to those from the much larger field data set (see also Dunham et al., 2011).

Shortening perpendicular to the kink bands across a sample is very small, averaging 0.70% for all samples (maximum 1.23%; Table 1). Shortening across individual kink bands as shown by $-e_{norm}$ is even smaller, averaging 0.14%. Individual samples generally have consistent shortening among transects, with more variation in those with larger tapered or intersecting kink bands (e.g. B10-1b, B10-F4; see electronic supplement). Kink bands with no intersections (e.g. those in Fig. 5 and non-intersecting kink bands in all samples) have consistent shortening values along strike, usually varying only within one tenth of a percent. Even for kink bands that bend but do not intersect (e.g. kink bands D and E in sample B10-F4; Fig. 5) there is very little change in shortening due to the bending of the band. Intersecting bands, however, show distinct changes in shortening near and at the points of intersection. For example, where kink bands H and I cross in an *X* intersection in sample B13-4T (see electronic supplement), shortening increases to 1.5% near the intersection from 0.3% near the top of the sample. At *Y* intersections (e.g. kink band K in sample B13-4T; Fig. 7), the shortening across each individual daughter strand (0.45% and 0.35%) is lower than the single parent strand (2%), but in most samples together accommodate similar shortening. For λ intersections, in each observed case the offshoot strand has significantly smaller shortening values than the primary strand (e.g. 0.12% for the offshoot and 0.8% for the primary kink band E in sample B10-1a; see electronic supplement). The offshoot strand generally also shows decreasing shortening along its strike as it diverges from the primary kink band.

Shortening is positively correlated with kink band density ($R = 0.73$; Table 2), and with maximum relief, gradient, and rotation angle (all R between 0.71 and 0.81; see Fig. 1 for definitions). Normalized shortening, however, shows no correlations with any other parameters. The steepening of the kink bands is also accompanied by a moderate increase in the curvature of the hinges ($R = 0.76$). A subset of kink bands (those in samples from outcrop B10) shows positive correlations between kink band density and maximum relief, plan width, and kinked width and negative correlations with average hinge width ($R = -0.80$). Unique to this subset of kink bands are correlations between mean curvature of the kink band hinges and gradient (R-0.73) as well as rotation angle ($R = 0.81$). There is no significant correlation between spacing of kink bands and any other measured variables (e.g. width, relief, curvature).

5. Discussion and conclusions

The curvature analyses presented here provide important insights on the geometry of kink bands in the third dimension and the relationships between metric parameters. The observations from digital micro-topography and calculated curvature provide a more detailed and precise characterization of kink bands than is possible in the field. The ability to quantify the gradient of kink bands and tightness of hinges and to obtain more accurate measurements of relief and width provides important information to understand how strain is localized within kink bands and their intersections.

Table 2
Correlation coefficient (R) matrix for 33 transects on 6 samples across the full length of the sample.

	−e	$-e_{norm}$[a]	D_{kb}	Relief (max)	Relief (avg)	Plan width (max)	Plan width (avg)	Kmean (max)	Kmean (avg)	Kinked width[b] (max)	Kinked width[b] (avg)	Hinge width (max)	Hinge width (avg)	Spacing (max)	Spacing (avg)	Gradient (max)	Gradient (avg)	Rotation angle[c] (max)
$-e_{norm}$[a]	–																	
Dkb	**0.734**	−0.374																
Relief (max)	**0.800**	0.068	0.621															
Relief (avg)	0.690	0.695	0.131	–														
Plan width (max)	0.419	−0.387	0.654	0.530	0.179													
Plan width (avg)	0.179	0.227	0.100	0.081	0.503	–												
Kmean (max)	0.468	−0.140	0.374	0.369	0.223	0.295	−0.150											
Kmean (avg)	0.133	0.161	−0.162	0.126	0.187	−0.183	−0.503	–										
Kinked width[b] (max)	0.465	−0.364	0.669	–	–	–	–	0.328	−0.135									
Kinked width[b] (avg)	0.238	0.282	0.110	–	–	–	–	−0.117	−0.459	–								
Hinge width (max)	0.035	−0.257	−0.017	0.308	0.056	0.307	−0.098	0.160	0.256	0.324	−0.091							
Hinge width (avg)	−0.509	0.286	**−0.773**	−0.448	−0.037	−0.395	−0.079	−0.180	0.263	−0.403	−0.081	–						
Spacing (max)	−0.434	−0.301	−0.293	−0.230	−0.323	−0.234	−0.562	0.037	0.413	−0.220	−0.570	0.317	0.187					
Spacing (avg)	−0.628	0.413	**−0.913**	−0.553	−0.049	−0.656	−0.189	−0.269	0.292	−0.668	−0.186	−0.044	0.675	–				
Gradient (max)	**0.719**	−0.077	0.586	–	–	–	–	0.632	0.179	0.416	0.072	0.126	−0.403	−0.341	−0.519			
Gradient (avg)	0.235	0.094	−0.014	–	–	–	–	0.365	0.496	−0.122	−0.367	0.166	−0.022	0.157	0.026	–		
Rotation angle[c] (max)	**0.812**	0.110	0.594	–	–	–	–	0.679	0.325	0.356	0.086	0.012	−0.388	−0.296	−0.412	–	–	
Rotation angle[c] (avg)	0.390	0.505	−0.116	–	–	–	–	0.370	**0.764**	−0.287	−0.338	0.068	0.123	0.273	0.298	–	–	–

Correlations with $R^2 > 0.5$ are indicated in bold and highlighted. Dashes denote non-correlatable pairs (same variable or directly calculated).

[a] Shortening normalized to number of bands.

[b] Calculated from relief and plan width.

[c] Calculated from kinked and plan widths.

Kink band measurements derived from the curvature analyses show relationships that are consistent with those seen in the field, and add several new parameters that are not measurable in the field. These observations give insight into the evolution of the kink bands. The strong correlation between maximum relief and shortening, and maximum rotation angle and shortening, support rotation as a mechanism for kinking: as bands rotate, they increase in relief and accommodate more shortening. In individual kink bands, curvature is highest in the hinges, as expected for tight folding of a planar surface. Hinge curvature increases as the rotation angle increases, and is weakly negatively correlated with plan width. Decreasing plan width with increasing rotation and hinge curvature is consistent with progressive rotation of the kinked limb and tightening of the hinges. The observed correlation thus adds additional support to the interpretation that fixed hinge or hybrid rotational mobile hinge kinematics describes the evolution of these kink bands (Dunham et al., 2011).

The geometry of kink bands in the third dimension is described more completely by using geometric curvature. The combination of gradient, total curvature, and geologic curvature maps allows for more precise mapping of kink band trends and geometry of individual kink bands or strands at complicated intersections than is possible in the field. However, the mechanisms by which kink bands intersect, merge, or split are still not well understood. The variability of kink band trends on the foliation surface make it likely that two kink bands trending at high angles to each other will cross in an *X*-type intersection, with one kink band kinking the other. The symmetrical geometry of Y-type intersections suggests that splitting of one kink band as it propagates is a possible scenario for the formation of such geometries; however, there is no visible control on the location of the intersections. The behavior of kink bands in λ-type intersections is puzzling, and no clear mechanism exists to explain how one hinge may split while the other remains continuous. Understanding the mechanisms or behavior of intersecting kink bands as they propagate requires further study. Deformation experiments that allow direct observation of kink band evolution in the third dimension could provide valuable information on the controls of complicated kink band geometries.

More generally, curvature analysis on kink bands demonstrates that even small topographic features can be successfully characterized by differential geometry. Curvature analysis allows for rapid identification of the surface shape via mean, total, and geologic curvature as well as direct comparison among individual structures. Geometric curvature analyses are a valuable tool for describing the curving and intersecting geometry of kink bands on the foliation surface and for extracting information on the strain accommodated by kink bands. The quantitative descriptions extracted permit statistical evaluation of correlations among geometric attributes of the kink bands. The techniques outlined here can be applied to broader scans of outcrops containing kink bands and automated, providing abundant observations of the three-dimensional geometry of these mesoscale structures. Such an approach may ultimately aid in illuminating the three-dimensional mechanics of kink bands.

Acknowledgments

We thank: Mark Pearce and Ian Alsop for thoughtful reviews that helped improve this manuscript; Meghan Hallam and Samuel Bruno for field assistance; property owners on Samish Island for access to outcrops; Derek Yip-Hoi of WWU's Electronics Engineering Technology Department for training and access to the FARO arm scanner; and Jackie Caplan-Auerbach of WWU's Geology Department for assistance with MATLAB coding. Funding was provided by a Geological Society of America Student Research Grant, Western Washington University Research and Sponsored Programs, Western Washington University Geology Department, and University of Washington Earth and Space Sciences.

Appendix. Supplementary data

Supplementary data related to this article can be found online at doi:10.1016/j.jsg.2012.01.003.

References

Bergbauer, S., Pollard, D.D., 2003. How to calculate normal curvatures of sampled geological surfaces. Journal of Structural Geology 25, 277–289.
Bergbauer, S., Pollard, D.D., 2004. A new conceptual fold-fracture model including prefolding joints, based on the Emigrant Gap anticline, Wyoming. Geological Society of America Bulletin 116 (3/4), 294–307.
Brown, E.H., 1986. Geology of the Shuksan Suite, North Cascades, Washington, U.S.A. Geological Society of America Memoir 164, 143–154.
Dewey, J.F., 1965. Nature and origin of kink bands. Tectonophysics 1 (6), 459–494.
Dunham, R.E., 2010. Kink band development in the Darrington Phyllite on Samish Island, northwestern Washington. M.S. thesis, Western Washington University.
Dunham, R.E., Crider, J.G., Burmester, R.F., Schermer, E.R., Housen, B.A., 2011. Geometry, microstructures, and magnetic fabrics of kink bands in the Darrington Phyllite, northwestern Washington, USA: processes within fixed-hinge kinking. Journal of Structural Geology 33, 1627–1638.
Gallagher, M.P., Brown, E.H., Walker, N.W., 1988. A new structural and tectonic interpretation of the western part of the Shuksan blueschist terrane, northwestern Washington. Geological Society of America Bulletin 100, 1415–1422.
Haugerud, R.A., 1980. The Shuksan Metamorphic Suite and Shuksan Thrust, Mt. Watson area, North Cascades, Washington. M.S. thesis, Western Washington University.
Haugerud, R.A., Morrison, M.L., Brown, E.H., 1981. Structural and metamorphic history of the Shuksan Metamorphic Suite in the Mount Watson and Gee point areas, North Cascades, Washington. Geological Society of America Bulletin 92, 374–383.
Hobson, D.M., 1973. The origin of kink bands near Tintagel, North Cornwall. Geological Magazine 100 (2), 133–144.
Jones, M.A., 1999. Geologic framework for the Puget Sound aquifer system, Washington and British Columbia. U.S. Geological Survey Professional Paper 1424-C.
Kirschner, D.L., Teixell, A., 1996. Three-dimensional geometry of kink bands in slates and its relationship with finite strain. Tectonophysics 262, 195–211.
Lamb, R.M., 2000. Structural and tectonic history of the eastern San Juan Islands, Washington. M.S. thesis, Western Washington University.
Lisle, R.J., 1994. Detection of zones of abnormal strains in structures using Gaussian curvatures analysis. AAPG Bulletin 78 (12), 1811–1819.
Lisle, R.J., Robinson, J.M., 1995. The Mohr circle for curvature and its application to fold description. Journal of Structural Geology 17, 739–750.
Lisle, R.J., Toimil, N.C., 2007. Defining folds on three-dimensional surfaces. Geology 35 (6), 519–522.
Lisle, R.J., Toimil, N.C., Aller, J., Bobillo-Ares, N., Bastida, F., 2010. The hinge lines of non-cylindrical folds. Journal of Structural Geology 32, 166–171.
Misch, P., 1966. Tectonic evolution of the northern Cascades of Washington State; A west-Cordilleran case history. Canadian Institute of Mining and Metallurgy 8, 101–148.
Mynatt, I., Bergbauer, S., Pollard, D.D., 2007. Using differential geometry to describe 3D folds. Journal of Structural Geology 29 (7), 1256–1266.
Paterson, M.S., Weiss, L.E., 1966. Experimental deformation and folding in phyllite. Geological Society of America Bulletin 77, 343–374.
Pearce, M.A., Jones, R.R., Smith, S.A.F., McCaffrey, K.J.W., Clegg, P., 2006. Numerical analysis of fold curvature using data acquired by high-precision GPS. Journal of Structural Geology 28, 1640–1646.
Ramsay, J.G., 1967. Folding and Fracturing of Rocks. McGraw-Hill, New York, p. 568.
Ritchie, J.C., 1995. Airborne laser altimeter measurements of landscape topography. Remote Sensing of Environment 53, 91–96.
Schermer, E.R., Gillaspy, J.R., Lamb, R., 2007. Arc-parallel extension and fluid flow in an ancient accretionary wedge: The San Juan Islands, Washington. Geological Society of America Bulletin 119, 753–767.
Stecchi, F., Antonellini, M., Gabbianelli, G., 2009. Curvature analysis as a tool for subsidence-related risk zones identification in the city of Tuzla (BiH). Geomorphology 107, 215–316.
Stewart, K.G., Alvarez, W., 1991. Mobile-hinge kinking in layered rocks and models. Journal of Structural Geology 13 (3), 243–259.
Stewart, S.A., Podolski, R., 1998. Curvature analysis of gridded geological surfaces. In: Coward, M.P., Daltaban, T.S., Johnson, H. (Eds.), Structural Geology in Reservoir Characterization. Geological Society, London, Special Publications, vol. 127, pp. 133–147.
Verbeek, E.R., 1978. Kink bands in the Somport slates, west-central Pyrenees, France and Spain. Geological Society of America Bulletin 89, 814–824.
Weiss, L.E., 1980. Nucleation and growth of kink bands. Tectonophysics 65, 1–38.
Yilmaz, H.M., 2007. The effect of interpolation methods in surface definition: an experimental study. Earth Surface Processes and Landforms 32, 1346–1361. doi:10.1002/esp.1473.